doi:10.1016/j.jmb.2010.01.063 J. Mol. Biol. (2010) 397, 814–825

JMB

Available online at www.sciencedirect.com

ScienceDirect

ELSEVIER

Mechanistic Insights into Ferredoxin–NADP(H) Reductase Catalysis Involving the Conserved Glutamate in the Active Site

Verónica I. Dumit[1,2]†, Timm Essigke[1]†, Néstor Cortez[2] and G. Matthias Ullmann[1]*

[1]*Structural Biology/ Bioinformatics, University of Bayreuth, Universitätsstr. 30, BGI, 95447 Bayreuth, Germany*

[2]*Instituto de Biología Molecular y Celular de Rosario, Universidad Nacional de Rosario, Suipacha 531, S2002LRK Rosario, Argentina*

Received 28 October 2009; received in revised form 26 January 2010; accepted 27 January 2010
Available online 2 February 2010

Plant-type ferredoxin–NADP(H) reductases (FNRs) are flavoenzymes harboring one molecule of noncovalently bound flavin adenine dinucleotide that catalyze reversible reactions between obligatory one-electron carriers and obligatory two-electron carriers. A glutamate next to the C-terminus is strictly conserved in FNR and has been proposed to function as proton donor/acceptor during catalysis. However, experimental studies of this proposed function led to contradicting conclusions about the role of this glutamate in the catalytic mechanism. In the present work, we study the titration behavior of the glutamate in the active site of FNR using theoretical methods. Protonation probabilities for maize FNR were computed for the reaction intermediates of the catalytic cycle by Poisson–Boltzmann electrostatic calculations and Metropolis Monte Carlo titration. The titration behavior of the highly conserved glutamate was found to vary depending on the bound substrates NADP(H) and ferredoxin and also on the redox states of these substrates and the flavin adenine dinucleotide. Our results support the involvement of the glutamate in the FNR catalytic mechanism not only as a proton donor but also as a key residue for stabilizing and destabilizing reaction intermediates. On the basis of our findings, we propose a model rationalizing the function of the glutamate in the reaction cycle, which allows reinterpretation of previous experimental results.

Keywords: photosynthesis; electron/proton transfer; avoprotein; electrostatic calculations; pH titration behavior

Edited by D. Case

Introduction

Plant-type ferredoxin–NADP(H) reductases (FNRs) constitute a family of monomeric enzymes harboring one molecule of noncovalently bound flavin adenine dinucleotide (FAD) as prosthetic group.[1–4] FNRs were found in chloroplasts, non-photosynthetic plastids, apicoplasts, cyanobacteria, and phototrophic and heterotrophic bacteria.[3,5] They catalyze reversible electron transfer between the iron–sulfur protein ferredoxin (Fd) or flavin-mononucleotide-containing flavodoxin and NADP(H):

$$2\mathrm{Fd}\left(\mathrm{Fe}^{2+}\right)+\mathrm{NADP}^{+}+\mathrm{H}^{+}\rightleftharpoons 2\mathrm{Fd}\left(\mathrm{Fe}^{3+}\right)+\mathrm{NADPH} \quad (1)$$

In chloroplasts and cyanobacteria, FNR provides the NADPH necessary for photosynthetic CO_2 assimilation. Remarkably, FNR is able to transfer electrons between one-electron carriers (Fd or flavodoxin) and two-electron carriers ($NADP^+$ and NADPH) involving its redox cofactor FAD. The flavin can adopt three different redox forms as the oxidized quinone form (FAD), the one-electron reduced semiquinone radical form ($FADH^{\cdot}$), and the fully reduced quinol form ($FADH_2$).[6]

The accepted mechanism of electron transfer from reduced Fd to $NADP^+$ follows a compulsory ordered pathway involving the formation of a ternary complex, with $NADP^+$ acting as the leading

*Corresponding author. E-mail address: Matthias.Ullmann@uni-bayreuth.de.

† V.I.D. and T.E. contributed equally to this work.

Abbreviations used: FNR, ferredoxin–NADP(H) reductase; FAD, flavin adenine dinucleotide; Fd, ferredoxin; PDB, Protein Data Bank; MC, Monte Carlo.

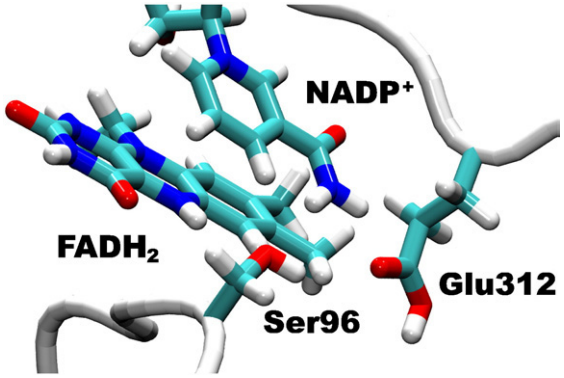

Fig. 1. Active site of FNR, including the isoalloxazine ring of $FADH_2$, the nicotinamide ring of $NADP^+$, and the side chains of Glu312 and Ser96. Intermediate VII of the catalytic cycle (Fig. 4) is depicted. The figure was prepared using the program VMD.[11,12]

substrate.[7,8] In both plant and bacterial FNRs, the recognition of $NADP^+$ includes a sequence of steps in which it is bound first in a nonproductive manner through the 2′-P-AMP moiety.[9,10] Then, the bound $NADP^+$ and the proximal regions of the protein undergo structural rearrangements, leading to a tightly bound $NADP^+$.[9,10] The displacement of the C-terminal tyrosine of FNR is suggested to be the final step, which allows nicotinamide to approach the flavin for hydride transfer. The movement of this residue appears to be essential for catalysis.[5,10] Eventually, electron transfer from reduced Fd to FAD occurs, yielding FADH·. Oxidized Fd is released from the complex. Thus, a second reduced Fd can reduce FADH· to its quinol form. Only after $FADH_2$ has been formed is $NADP^+$ converted into NADPH via hydride transfer. The N-5 atom of the flavin is in hydrogen-bond distance to a serine, which in turn is in hydrogen-bond distance to the carboxylate of a conserved glutamate (Fig. 1). Since this glutamate residue is exposed to the solvent, it has been proposed to be responsible for transferring protons from the external medium to the buried N-5 atom of the isoalloxazine via the serine.[13]

Evidence that the glutamate is involved in the catalytic mechanism of FNR was obtained by Kurisu *et al.*, who found a significant difference between the crystal structure of the Fd-bound FNR and the crystal structure of the free FNR from maize: In the structure of the FNR–Fd complex, Glu312 forms a hydrogen bond with Ser96, while there is no hydrogen bond in the structure of free FNR.[14] A possible function of the glutamate as proton donor/acceptor was previously investigated by Medina *et al.*[15] and Aliverti *et al.*[16] However, both groups drew contradictory conclusions about its role in the mechanism. While Aliverti *et al.*[16] could not see evidence for the function of Glu312 as proton donor/acceptor in their enzymatic assays that do not involve Fd, Medina *et al.*[15] speculated about the role of Glu312 as proton donor, especially in the presence of the physiological electron transfer partner Fd.

In this work, we study the role of the glutamate in the active site of FNR during catalysis. Protonation probability calculations of all titratable residues in free FNR and in its complexes with NADP(H) and Fd indicate that the conserved glutamate is involved in the enzymatic mechanism as proton donor/acceptor. We propose a model for the reaction mechanism that is consistent with the data of Medina *et al.*[15] and Aliverti *et al.*[16]

Results and Discussion

In this work, we study the enzymatic mechanism of FNR, in particular the role of the conserved glutamate in the active site as possible proton donor/acceptor. The protonation and deprotonation of Glu312 (maize leaf FNR amino acid numbering is used throughout this work) in intermediates of the catalytic cycle were incorporated into the mechanism of Batie and Kamin according to our calculations.[7] Glu312 could be responsible for protonating the N-5 atom of the isoalloxazine ring of the flavin via the bridging Ser96. Protein sequence alignments for plant and bacterial FNRs showed that Glu312 and Ser96 are conserved in all sequences (Supporting Information). This strict conservation indicates that both residues could play an important role in the catalytic mechanism of the enzyme. An alignment (Table 1) based on the crystal structures available for different organisms showed that not only the sequence position but also the three-dimensional position of Glu312 and Ser96 are conserved in bacterial and plastidic FNRs.

Table 1. Sequence alignment based on a structural superposition of FNRs showing the conserved serine and glutamate in the reaction center

Organism	Sequence alignment			
R. capsulatus	59>	--GKPIMRAYSIASPAW-	254>	ANSEPREFVVEKAFVGEGI
A. vinelandii	46>	--GRPLMRAYSIASPNY-	242>	RMGEPGDYLIERAFVEK--
E. coli	44>	----RVQRAYSYVNSP--	235>	LRRRPGHMTAEHYW-----
Anabaena	70>	NGKPEKLRLYSIASTRHG	291>	DLKKAGRWHVETY-----
P. falciparum	63>	----RCARLYSISSSNN-	304>	DEKKKKRVHVEVY-----
Maize root	84>	PGAPQNVRLYSIASTRYG	304>	QLKKNKQWHVEVY-----
Maize leaf	86>	NGKPHKVRLYSIASSAIG	302>	QLKRGDQWNVEVY-----
Spinach	86>	NGKPHKLRLYSIASSALG	302>	QLKKAEQWNVEVY-----
Pea	80>	NGKPHKLRLYSIASSAIG	296>	TLKKAEQWNVEVY-----
Paprika	135>	GKPHKLRLYSIASSALG	350>	QLKKAEQWNVEVY-----

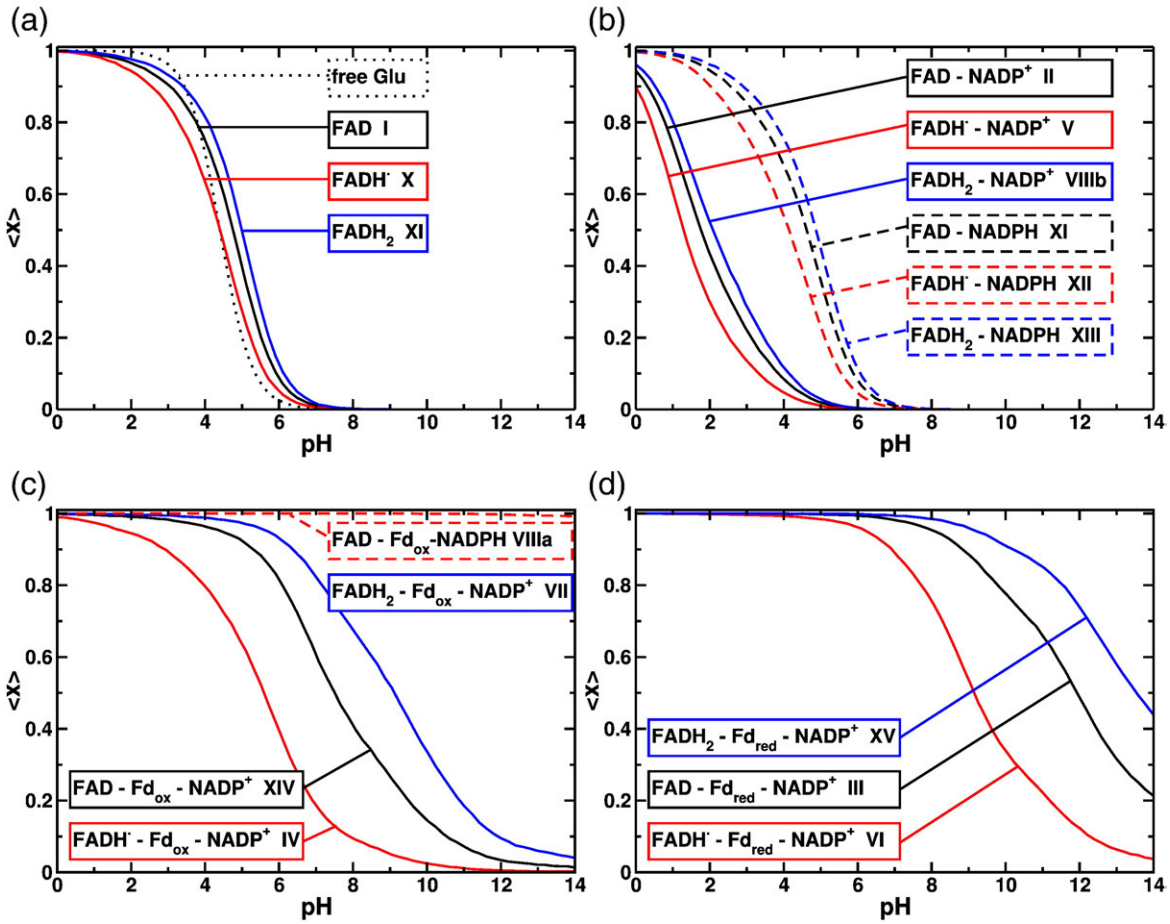

Fig. 2. Protonation probability curves of Glu312 in dependence of pH: (a) water and free FNR; (b) binary complex of FNR with NADP(H); (c) ternary complex of FNR with NADP(H) and Fd_{ox}; and (d) ternary complex of FNR with NADP(H) and Fd_{red}. The error in protonation probability from different MC runs is less than 1%.

Titration behavior of Glu312

We calculated the protonation probability of all titratable residues of free maize FNR and its complexes with NADP(H) and Fd. Figure 2 shows the protonation probability of Glu312 in FNR calculated for different redox states. These curves are referred to as titration curves from now on.

The protonation energy of an amino acid residue inside a protein can be shifted compared to its value in aqueous solution by several contributions: (i) changes in solvation energy ($\Delta\Delta G_{Born}$); (ii) interac-

Table 2. Protonation energy $\Delta G_{TR,7}$ and its contributions: $\Delta\Delta G_{Born}$, $\Delta\Delta G_{back}$, and $\Delta G_{TR,7}^{inter}$ of Glu312 in different steps of the reaction cycle, calculated at pH 7.0 (kcal/mol)

FNR complex	$\Delta G_{TR,7}$	$\Delta\Delta G_{Born}$	$\Delta\Delta G_{back}$	$\Delta G_{TR,7}^{inter}$	Intermediate
FAD	2.8	−2.2	0.7	0.6	I
FAD $NADP^+$	4.9	−2.2	2.8	0.7	II
FAD $NADP^+$ Fd_{red}	−2.5	−11.2	3.6	1.4	III
$FADH^·$ $NADP^+$ Fd_{ox}	1.0	−11.2	7.1	1.4	IV
$FADH^·$ $NADP^+$	5.3	−2.2	3.2	0.7	V
$FADH^·$ $NADP^+$ Fd_{red}	−1.3	−11.2	4.7	1.4	VI
$FADH_2$ $NADP^+$ Fd_{ox}	−1.0	−11.2	5.2	1.3	VII
FAD NADPH Fd_{ox}	−5.9	−11.2	0.2	1.4	VIIIa
$FADH_2$ $NADP^+$	4.7	−2.2	2.5	0.7	VIIIb
FAD NADPH	2.8	−2.2	0.7	0.7	IX
$FADH^·$	3.1	−2.2	1.0	0.6	X
$FADH_2$	2.5	−2.2	0.4	0.6	XI
$FADH^·$ NADPH	3.1	−2.2	1.0	0.6	XII
$FADH_2$ NADPH	2.5	−2.2	0.4	0.6	XIII
FAD $NADP^+$ Fd_{ox}	−0.3	−11.2	5.9	1.3	XIV
$FADH_2$ $NADP^+$ Fd_{red}	−3.2	−11.2	2.9	1.4	XV

$\Delta G_{TR,7}$ is based on the Tanford–Roxby equation to approximate the titration curves of proteins.

tion with permanent charges and dipoles of the protein ($\Delta\Delta G_{back}$); and (iii) interaction with other titratable residues ($\Delta G^{inter}_{TR,7}$). Table 2 lists the protonation energy of Glu312 at pH 7.0 in different intermediates, as well as the above listed contributions (the protonation energies of additional redox states are given in Supporting Information). The Roman numbering introduced in Table 2 is used to identify the different intermediates throughout the study. The titration curves of Glu312 in FNR with FAD (I), FADH· (X), and $FADH_2$ (XI) are similar to that of a free glutamate residue (Fig. 2a).

The titration curves of FNR with bound $NADP^+$ (II, V, and VIII b; Fig. 2b) are shifted towards lower pH values and, consequently, the protonation energy of Glu312 at pH 7.0 becomes more positive. Instead, the titration curves of FNR with bound NADPH (V, XII, and XIII) are not significantly shifted due to the neutrality of the nicotinamide ring.

The titration curves of Glu312 in the ternary complex (FNR, Fd, and NADP(H)) are shifted to higher pH values compared to the titration curve of the residue in solution (Fig. 2c), leading to more negative values of protonation energies (Table 2). Here, Glu312 is likely to be protonated (i.e., the protonation energy in Table 2 is negative) even in complexes with $NADP^+$ (III, VI, VII, XIV, and XV), with one exception—the redox state FADH·–$NADP^+$–Fd_{ox} (IV). The complexes with NADPH show very high deprotonation energies between 4.8 and 8.7 kcal/mol (see Supporting Information; 5.9 kcal/mol for intermediate VIIIa). This large shift is mainly caused by a change in $\Delta\Delta G_{Born}$, which can be explained by a conformational change in Glu312 in comparison to the free FNR and shielding due to Fd binding. Due to the strong interaction with the [Fe2–S2] cluster, the deprotonation energy of Glu312 is sensitive to the redox state of Fd: Fd_{red} (III, VI, and XV) stabilizes protonated Glu312 even more (change in interaction energy, −6.2 kcal/mol) than Fd_{ox} (XIV, IV, and VII; change in interaction energy, −3.9 kcal/mol). In the ternary complex (VIIIa), the protonated form of Glu312 is even more stabilized after the hydride transfer because of the neutralization of the positive charge of $NADP^+$. Interestingly, the relative order of the titration curves of Glu312 in the presence of the three forms of the flavin (FAD, FADH·, and $FADH_2$) is the same in FNR and all its complexes. The titration curve of Glu312 in structures with the semiquinone form is shifted towards lower pH values, and the reduced form is shifted towards higher pH values compared to the oxidized form. Considering that the three forms of the flavin are electroneutral, this effect can be attributed to the direction of higher multipoles of the isoalloxazine ring. The deprotonated Glu312 stabilizes the charge distribution of the N-5 protonated semiquinone form. Figure 3 shows the electrostatic potential of the isoalloxazine ring in the three redox forms.

In summary, the titration curves of Glu312 in Fig. 2 are influenced by the binding of Fd and NADP(H), as well as by the redox states of Fd, NADP(H), and FAD. Fd binding has the largest effect due to the desolvation of the active site.

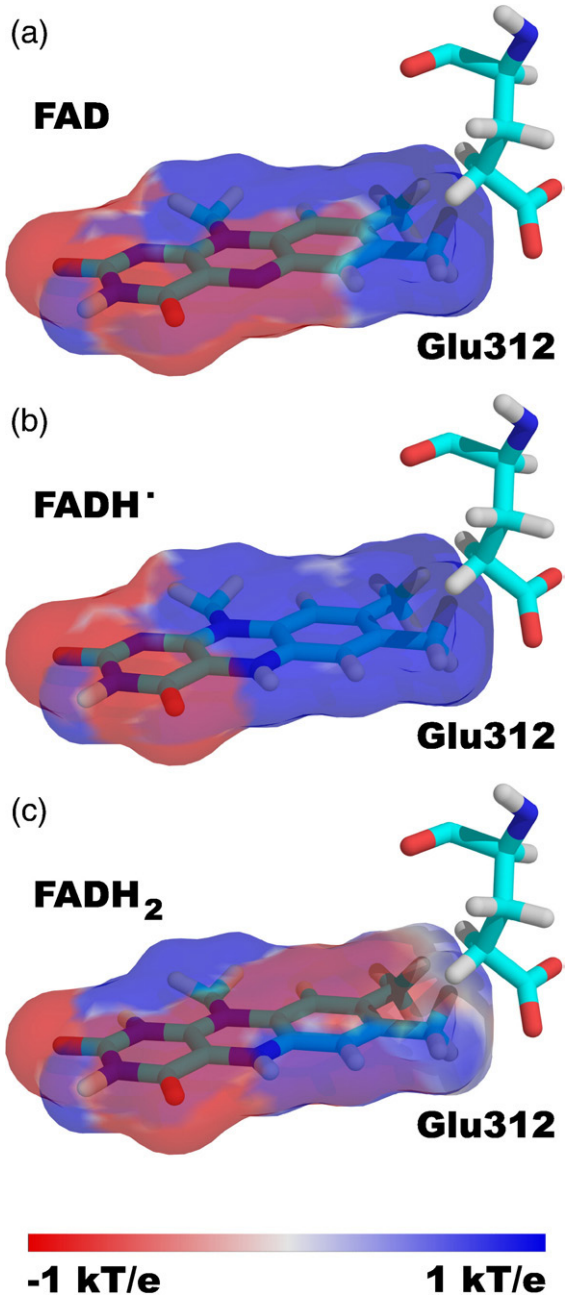

Fig. 3. Electrostatic potential of the isoalloxazine ring of the flavin in its three neutral redox forms (a) FAD, (b) FADH· and (c) $FADH_2$. The electrostatic potential is mapped in the range of ±1 kT/e onto the molecular surface of the flavin according to the color bar. The semiquinone form has a clear positive potential (blue) interacting favorably with the deprotonated Glu312, while the negative potential (red) is located at the opposite end of the molecule. The other two redox forms have a negative potential closer to Glu312. Therefore, the semiquinone form is stabilized by FNR in intermediate V of Fig. 4. The figure was prepared using various programs.[17–19]

Proposed catalytic cycle of FNR

Based on our calculations, we included the participation of Glu312 in a previously proposed catalytic cycle.[7] Intermediates are referenced by roman numbers, and reaction steps between the intermediates are identified by arabic numbers, as shown in Fig. 4. We discuss the cycle assuming that the reactions would occur at pH 7.0.

Formation of the semiquinone of flavin

Following the model of Batie and Kamin, we assume $NADP^+$ to be the leading substrate in the catalytic cycle.[7] According to our calculations, Glu312 is deprotonated in the free enzyme (I). Binding of $NADP^+$ (II) does not alter the protonation form of Glu312. Interaction of FAD–$NADP^+$ with Fd_{red} (III) leads to the protonation of Glu312, as indicated by the shifted titration curve of this intermediate (Fig. 2c).

After the transfer of the electron from Fd to the flavin (IV), the deprotonated Glu312 is favored by −1.0 kcal/mol in the ternary complex. The deprotonation of Glu312 is remarkable because in all other complexes with Fd, the glutamate is protonated. Taking into account that, in plant FNRs, the anionic red flavin semiquinone is not observed and that the flavin is not solvent accessible when Fd is bound,[14] the proton released from Glu312 could be responsible for neutralizing the flavin. From the titration calculations, we estimate that the free energy of the proton transfer from Glu312 to the semiquinone of the flavin is about −2.4 kcal/mol; thus, the proton will be transferred from Glu312 to N-5 of the flavin. Moreover, taking the geometric orientation of Glu312, Ser96, and the flavin into account (Fig. 1), a transfer via Ser96 seems to be likely.

The negative charge of the then deprotonated Glu312 destabilizes the complex with the negatively charged Fd. Considering the different redox forms of the iron–sulfur center of Fd and the flavin, and the different protonation forms of Glu312, the electrostatic interaction energy with Fd changes from −5.1 kcal/mol for intermediate III to 0.6 kcal/mol for intermediate IV (Table 3), which means that the FNR–Fd complex is 5.7 kcal/mol less stable.

Thus, we propose two functions of Glu312 deprotonation: First, the proton transfer from Glu312 to the flavin allows a fast protonation of the isoalloxazine ring, and, second, the proton transfer from Glu312 to flavin helps to expel the

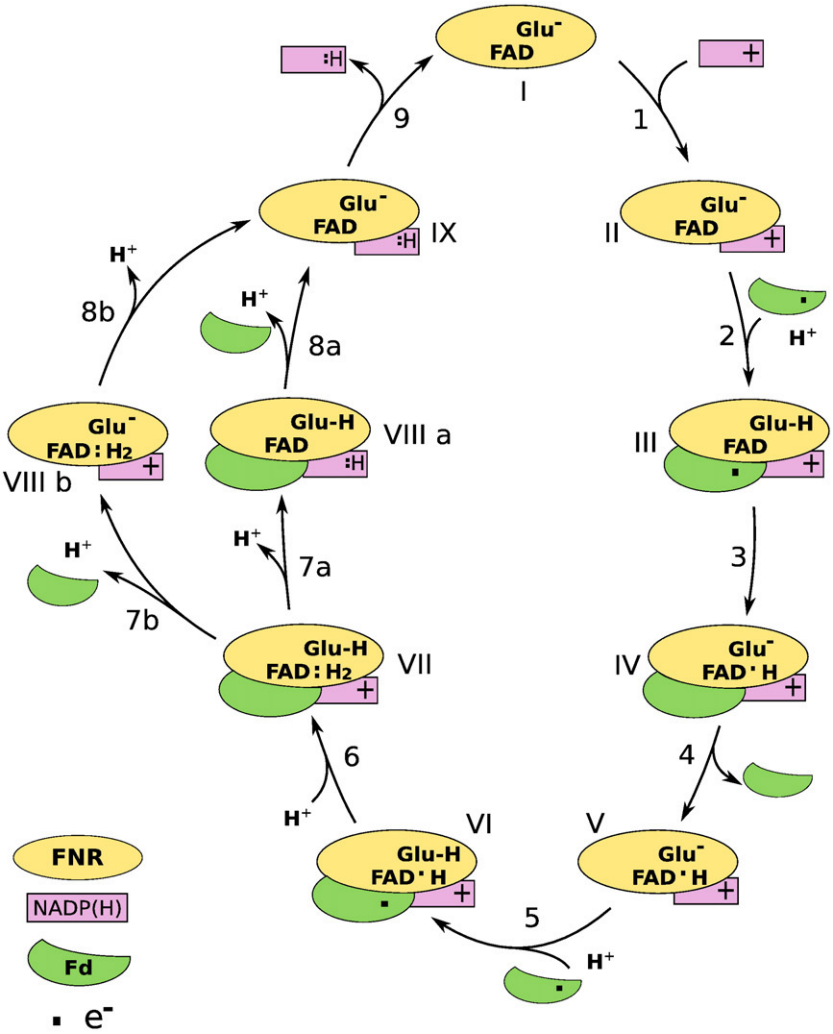

Fig. 4. Catalytic mechanism of FNR. The protonation form of Glu312 is indicated. The steps show the electron and proton flow during catalysis. (1) FNR–$NADP^+$ complex formation (Glu312 remains deprotonated during this reaction). (2) Binding of Fd_{red} and Glu312 protonation. (3) Electron transfer from Fd_{red} to FAD, accompanied by proton transfer from Glu312 to the cofactor. (4) Fd_{ox} release. (5) Second Fd_{red} binding and Glu312 protonation. (6) Second electron transfer to FAD. (7a) Hydride transfer from $FADH_2$ to $NADP^+$. (8a) Fd_{ox} release and Glu312 deprotonation. (9) NADPH release from the FNR–NADPH complex. (7b–8b) Alternative hydride transfer where Fd_{ox} dissociates before $NADP^+$ reduction.

Table 3. Sum of interaction energies between the flavin, NADP(H), and Glu312 in FNR and the iron–sulfur center of Fd for intermediates of the catalytic cycle

	Interaction partner		Interaction energy (kcal/mol)	
Intermediate	FNR	Fd	Protonated Glu312	Deprotonated Glu312
III	FAD $NADP^+$ Glu312	Fd_{red}	**−5.1**	1.1
IV	FADH· $NADP^+$ Glu312	Fd_{ox}	−3.3	**0.6**
VI	FADH· $NADP^+$ Glu312	Fd_{red}	**−5.1**	1.1
VII	$FADH_2$ $NADP^+$ Glu312	Fd_{ox}	**−2.4**	1.5
VIIIa	FAD NADPH Glu312	Fd_{ox}	**−1.3**	2.6

The interaction energies for the protonation form of Glu312 proposed in Fig. 4 are shown in boldface. The details of the calculations are explained in Change in Interaction Energy between FNR and Fd.

negatively charged Fd_{ox} from the complex. The FNR is now ready for reduction by a second Fd_{red}.

FADH· is stabilized in order to minimize unwanted side reactions, ensuring the catalytic function of FNRs as switch between one-electron carriers and two-electron carriers. As shown in Table 4, FADH· is only stabilized by the deprotonated Glu312, and not by a protonated Glu312 or by Ala in the E312A mutant. Our protonation probability calculations predict that Glu312 is deprotonated when Fd is not bound. We can therefore suggest a third function for Glu312, which is to stabilize the semiquinone state in the complex without Fd.

Formation of the quinol state of flavin

Binding of the second Fd_{red} has a similar effect as binding of the first Fd_{red} (i.e., Glu312 is protonated again (VI)). After the electron has been transferred to the flavin cofactor (step 6), the deprotonation energy of Glu312 decreases by 0.3 kcal/mol (VII), but Glu312 remains protonated according to our calculations. Mechanistically, it also seems unlikely that Glu312 transfers its proton to FADH·, since this proton would have to be transferred to N-1 of the isoalloxazine ring, which is about 11 Å away from the carboxylate of Glu312 (Fig. 1). Thus, Glu312 remains most likely protonated in this step. FADH· may take up a proton from solution to protonate N-1 of the isoalloxazine ring, which seems possible based on an inspection of the hydrogen-bond network.

Hydride transfer to $NADP^+$

Considering the geometrical arrangement (Fig. 1), it is plausible that the proton bound to N-5 of $FADH_2$, together with two electrons, is transferred to $NADP^+$, and the proton bound to N-1 is released to the solvent. The transfer may occur either as a concerted transfer of one proton and two electrons, or in a sequential manner. Our study investigates only the end states of this reaction. The exact mechanism of the hydride transfer that occurs over a very short distance is not investigated. It is argued that the release of Fd from FNR is a slow process, while hydride transfer is considered to be fast. Therefore, it is assumed that the hydride transfer occurs in the ternary complex.[4] We took into account the two possible reaction pathways for our calculations to provide new insights into the order of events between $NADP^+$ reduction and Fd release.

Our results indicate that Glu312 is deprotonated in the binary complex of FNR and $NADP^+$ (VI–IIb), but protonated in the ternary complex of FNR, NADPH, and Fd (VIIIa; Table 2). Calculations of the relative interaction energy of Fd_{ox} with FNR (Table 3) show that Fd is bound more strongly to FNR in the complex $FADH_2$–$NADP^+$–Fd_{ox} (VII) compared to FAD–NADPH–Fd_{ox} (VIIIa). This interaction energy difference is the first indication that Fd dissociates more likely after the hydride transfer (step 8a) than before the hydride transfer (step 7b).

The reaction energy for the transfer of a hydride between $FADH_2$ and $NADP^+$ is not favorable by 4.8 kcal/mol in solution.[20] The protein environment lowers this reaction energy to permit a transfer of the hydride to $NADP^+$. Calculations show that the hydride-transfer energy (Table 5) is lowered by 3.0 kcal/mol by the protein if Fd_{ox} is bound and Glu312 is protonated (step 7a). Instead, if Fd_{ox} is not bound and Glu312 is deprotonated, the energy for the hydride transfer is lowered by only 0.3 kcal/mol (step 8b). If Fd_{ox} is not bound and Glu312 is protonated, the hydride transfer reaction energy is lowered by 2.2 kcal/mol. However, this possibility seems unlikely, since 4.7 kcal/mol is required to protonate Glu312 in this intermediate (Table 2). Therefore, reduction of $NADP^+$ is highly unlikely when Fd is released first. Both protonated Glu312 and bound Fd_{ox} (VIIIa) are required for the enzyme to fulfill its catalytic function (step 7a).

In step 8a, the negatively charged Fd_{ox} is released from the complex because the interaction energy of NADPH and Fd_{ox} is 2.0 kcal/mol lower than that with $NADP^+$. Interestingly, the effect of the neutralization of the positive charge in the complex is

Table 4. Change in electrostatic interaction energy between the flavin in its different redox forms and residue 312 in wild type (protonated and deprotonated) and in E312A FNR forms

	Interaction energy (kcal/mol)	
	FAD→FADH·	FADH·→$FADH_2$
Glu312-H	0.1	−0.1
$Glu312^-$	−0.4	0.6
E312A	0.0	0.0

Calculations are based on the structure of intermediate V in Fig. 4.

Table 5. Shift in hydride transfer energies ΔG_{H-} from $FADH_2$ to $NADP^+$ and its contributions

			ΔG_{intr}		ΔG_{inter}		
Step	FNR complex	$\Delta\Delta G_{H-}$	$\Delta\Delta G_{Born}$	$\Delta\Delta G_{back}$	NADP/FAD	Other residues	Glu312
7a[a]	$Glu312^-$, Fd_{ox}	2.1	−10.2	7.3	0.7	−0.6	4.9
7a	Glu312-H, Fd_{ox}	−3.0	−10.2	7.3	0.7	−0.6	−0.2
8b	$Glu312^-$	−0.3	−9.4	7.4	0.8	−0.5	1.4
8b[a]	Glu312-H	−2.2	−9.4	7.4	0.8	−0.5	−0.5

Energy shift is split into contributions caused by shifts in the intrinsic energy ΔG_{intr} (desolvation effects $\Delta\Delta G_{Born}$ and interaction with non-titrating groups of the protein $\Delta\Delta G_{back}$) and energy shift due to interactions between titrating groups ΔG_{inter} (change in the interaction between FAD and NADP, change in the interaction between FAD/NADP and other titratable groups except for Glu312, and change in the interaction between FAD/NADP and Glu312). All calculations are performed at pH 7.0. Energies are given in kilocalories per mole.

[a] The protonation form of Glu312 differs from the one proposed in Fig. 4.

partially compensated for by the change in the dipole of the flavin, leading to an overall decrease in interaction energy of 1.1 kcal/mol (Table 3). Dissociation of Fd leads to a deprotonated Glu312 (IX), which helps to expel the formally three times negatively charged NADPH (step 9). The catalytic cycle is completed.

Discussion of previous experimental results

Calculations presented in this work support an active role for Glu312 during the catalytic cycle of FNR not only by stabilizing the semiquinone form of FAD but also as proton donor/acceptor in catalytic reactions.

Previous experimental results by Medina *et al.*[15] and Aliverti *et al.*[16] suggested the involvement of Glu312 in the stabilization of the semiquinone state of the enzyme, since photoreduction assays exhibited no semiquinone form for the E312A mutant FNR from *Anabaena*[15] and the spinach mutant FNR accumulated three times less FADH· relative to the wild-type protein.[16] The destabilization of semiquinone was also evident from the oxidase activity. When the native FNR is incubated with NADPH under aerobic conditions, a considerable amount of superoxide radical is formed by a two-phase process through a semiquinone intermediate state, while the mutant protein only produces H_2O_2 through a single-phase reaction, avoiding the semiquinone intermediate form.[15] In the diaphorase reaction, kinetic measurements can be made by using non-physiological small electron acceptors. The Glu312 mutant FNRs showed that no k_{cat} decreased relative to the wild-type enzyme when a two-electron acceptor was used (such as dichlorophenolindophenol or 2-(4-iodophenyl)-3-(4-nitrophenyl)-5-phenyl tetrazolium chloride). However, when a one-electron acceptor such as ferricyanide was used, the relative k_{cat} decreased by about 60%,[15,16] since the semiquinone intermediate must be formed. In the electron transfer reaction involving FNR and small artificial electron acceptors, Glu312 had no crucial function as proton donor/acceptor. In these reactions, Glu312 was deprotonated, since Fd is not bound and, thus, the large desolvation effect due to Fd binding, which leads to the protonation of Glu312, is missing. The stabilization of the semiquinone by the deprotonated Glu312 can be rationalized by the different electrostatic potentials of the flavin in its redox form and its interaction with Glu312. The semiquinone form needs to be stabilized in the free FNR (i.e., when Fd is not bound). In this intermediate, Glu312 is negatively charged and can stabilize the partially positively charged region around N-5 of the isoalloxazine ring (Fig. 3).

In reactions of FNR that involve Fd, the catalytic efficiency of FNR is largely impaired when Glu312 is mutated to an alanine. The performance of E312A mutants in the NADPH-dependent cytochrome *c* reductase reaction was even worse with respect to the wild-type FNR than in the diaphorase assay.[15,16] This reaction involves electron transfer from NADPH to Fd catalyzed by FNR and, subsequently, to cytochrome *c*. In another single-turnover experiment following the electron transfer between FNR and Fd, the mutant enzyme showed a significant decrease in catalysis compared to the wild-type FNR.[15] This remarkably decreased activity of the mutant proteins[15,16] indicates that Glu312 plays an additional role in catalysis besides stabilization of FADH· when Fd is present; it functions as a proton donor/acceptor once per catalytic cycle and destabilizes the FNR–Fd complex once the electron is transferred.

It was concluded[16] by single-turnover measurements that Glu312 is important in catalyzing the reductive half-reaction:

$$FNR_{ox} + NADPH + H^+ \rightleftharpoons NADP^+ + FNR_{red} \quad (2)$$

This reaction occurs in two steps in wild-type FNRs: formation of the charge-transfer complex $[FNR_{ox} - NADPH]^*$ and reduction of FAD by NADPH through hydride transfer:[7,8]

$$FNR_{ox} + NADPH \rightleftharpoons [FNR_{ox} - NADPH]^* \quad (3)$$

$$[FNR_{ox} - NADPH]^* + H^+ \rightleftharpoons [FNR_{red} - NADP^+] \quad (4)$$

In the experiments, the first phase is faster than the detection limits; therefore, only the rates of flavin reduction were determined for mutant and wild-type FNRs.[15,16] It was noted that the mutant protein

performed the reaction shown in Eq. (4) with significantly decreased efficiency. This finding can be explained by considering the importance of Glu312 in the hydride transfer process, as shown in Table 5. This reaction would occur through steps 8b–7b from the cycle in Fig. 4. Then, the crucial role of Glu312, which is deprotonated, is to favor the hydride transfer by stabilizing the positive charge of $NADP^+$. Glu312's function as proton donor/acceptor is only manifested in the presence of Fd.

Aliverti *et al.* observed that the relative activity of hydride transfer in the mutant protein is similar to the activity assayed through steady-state measurements with ferricyanide.[16] They concluded that the reductive half-reaction is therefore the one affected by this mutation. Based on their findings, they ruled out the involvement of Glu312 as proton donor/acceptor.[16] However, neither the diaphorase reaction nor the half-reductive reaction represents the physiological enzymatic cycle. The involvement of Glu312 was not directly proven by Medina *et al.*[15] However, they concluded that Glu312 functions as a proton donor/acceptor based on the lower electron transfer activity displayed by the E312A mutant of FNR, especially as observed in the experiments where Fd is used as substrate.

It is important to realize that many experiments investigating FNR activity involve non-physiological electron donors or acceptors. Moreover, catalytic reactions are often run in the opposite direction compared to physiological reactions, and conclusions drawn from these experiments may not always be transferable to the physiological cycle. From our calculations, we see that the binding of Fd has a pronounced effect on the catalysis of FNR. Results obtained from diaphorase reactions with small redox-active molecules cannot mimic desolvation effects due to Fd binding that seems to be important for the physiological reaction.

Conclusion

The role of a highly conserved glutamate residue in the active site of FNR was studied by continuum electrostatic computations. Protonation probability calculations were performed on different redox states of maize FNR and its binary and ternary complexes with Fd and NADP(H). The protonation energy of Glu312 varied over 14.6 kcal/mol for the complexes that we considered (Table 2; Supporting Information). We found that the protonation of active-site residues may change during catalysis not only due to chemical reactions but also due to the binding of reaction partners. The protonation energy of Glu312 is influenced by desolvation effects due to Fd binding and by the redox states of NADP(H), Fd iron–sulfur cluster, and flavin. The order of these influences reflects their importance. By arrangement of the complexes in the accepted catalytic cycle of FNR, the changes in the protonation form of Glu312 allowed us to propose an active role for this residue in the catalytic mechanism. Based on our calculations, we found the following functional roles for Glu312 in the catalytic cycle (Fig. 4): First, upon reduction of FAD to its semiquinone form by Fd, Glu312 deprotonates (step 3). Considering the geometric arrangement, it is likely that the proton is transferred from Glu312 via Ser96 to N-5 of the deprotonated semiquinone form of the flavin, allowing a fast protonation of the isoalloxazine ring. Second, after this proton–electron transfer, the deprotonated Glu312 destabilizes the binding of the strongly negatively charged Fd_{ox} and therefore promotes its dissociation (step 4). Third, the deprotonated Glu312 stabilizes the semiquinone state of the complex without Fd (V), therefore preventing side reactions of the radical before the second reduction step can occur. Only because of this property, can FNR function as a switch between one-electron carriers and two-electron carriers. Fourth, after the reduction of the semiquinone to $FADH_2$, the hydride transfer from $FADH_2$ to NADP+ is only energetically favorable if Glu312 is protonated and Fd is bound (step 7a). Fifth, a deprotonated Glu312 in the final reaction step helps to expel the formally three times negatively charged NADPH from the complex (step 9).

Our calculations allowed us to attribute functional roles to Glu312, which was assumed to be mechanistically important since the crystal structure of FNR was solved.[13]

Materials and Methods

Sequence alignment

FNR sequences from plant and bacterial FNR were aligned with CLUSTAL W.[21] The programs MultiProt[22] and Staccato[23] were used to obtain a reliable sequence alignment of FNRs based on structural information. Crystal structures of the FNRs from bacteria *Rhodobacter capsulatus*, *Azotobacter vinelandii*, and *Escherichia coli*;[24–26] from cyanobacterium *Anabaena*;[27] from protozoan *Plasmodium falciparum*;[28] and from plants spinach, pea, paprika, and maize (leaf and root isoforms)[13,14,29–31] were used [Protein Data Bank (PDB) IDs 2bgi, 1a8p, 1fdr, 1que, 2ok8, 1fnb, 1qg0, 1sm4, 1gaw, and 1jb9, respectively].

Structures for electrostatic calculations

All calculations were performed on maize FNR. We used PDB ID 1gaw (chain A) for the FNR alone and PDB ID 1gaq (chains A and B) for the FNR–Fd complex.[14] Complexes with NADP(H) were modeled based on the structure of the mutant Y308S of pea FNR co-crystallized with $NADP^+$ (PDB ID 1qfy; chain A).[29] The FNR structures of pea and maize were superimposed by matching the coordinates of the isoalloxazine ring using the Kabsch algorithm,[32] and the coordinates of NADP(H) were copied. In order to remove unfavorable Lennard–Jones interactions between nicotinamide and the protein, we energy minimized Thr172, Glu173, Leu274, Val313, and the C-terminal Tyr314 of FNR using a simulated annealing protocol. Since the N-terminus was not resolved crystallographically, we blocked the first resolved residue by an acetate group. The unresolved terminus should affect the titration behavior of the rest of the protein only marginally because

it is highly flexible and well solvated, and its charges are consequently well shielded. Hydrogens were placed using the HBUILD[33] routine of CHARMM.[34] The energy of the resulting structures was minimized, keeping all non-hydrogen atoms at fixed positions. For this optimization, all titratable groups were in their standard protonation form: acids (aspartate, glutamate, and C-terminus) were deprotonated, and bases (arginine, cysteine, histidine, lysine, tyrosine, and the N-terminus of Fd) were protonated. All water molecules and sulfate ions were removed from the structures after the modeling.

As a result of this structure preparation procedure, we obtained four coordinate sets: one for FNR (including the flavin), one of the complexes of FNR with NADP(H), one for the complex for FNR with Fd, and one for the complex of FNR with NADP(H) and Fd.

Atomic partial charges

Partial charges from the CHARMM27 force field[35] were used for amino acid residues. For NADP(H), the parameterization by Pavelites *et al.* was used.[36] Charges of the isoalloxazine ring of the flavin were computed by the RESP[37] method based on the results of DFT optimization (B3LYP) with Gaussian 03,[38] using a (6–311++g(2d,2p)) basis set for FAD, $FADH^{\cdot}$, $FADH^{-}$ and $FADH_2$ (charges in Supporting Information). Partial charges for the rest of the molecule were taken from analogous atoms in the NADP(H) parameterization. The iron–sulfur center of Fd and the side chains of the coordinating cysteines were geometry optimized with ADF[39,40] using a TZ2P(+) basis set and VWN[41] and PW91[42,43] exchange correlation functionals.[44] Charges were fitted by a CHELPG-like procedure (charges in Supporting Information).[45,46] The quantum chemical calculations were performed in vacuum starting from geometries obtained from the crystal structures. The coordinates of the atoms linking the iron–sulfur cluster to the protein were kept fixed similar to previous calculations.[47] The non-hydrogen atom RMSD of the optimized cluster compared to the crystal structure is 0.16 Å for the oxidized cluster and 0.18 Å for the reduced cluster.

We considered two charge forms for all arginine, aspartate, glutamate, lysine, tyrosine, and non-iron-coordinating cysteine in FNR and Fd. The charges for the protonated form of glutamate and aspartate and for the deprotonated form of lysine and arginine were symmetrized. The nicotinamide ring of NADP(H) and the iron–sulfur center of Fd were represented by two charge forms. Three charge forms were used for the isoalloxazine ring of the flavin, and four charge forms (doubly protonated, ε protonated, δ protonated, and deprotonated) were used for the histidine side chain.

Theoretical framework for the computation of protonation probabilities

Protonation probabilities were obtained by combining Poisson–Boltzmann electrostatic calculations with Metropolis Monte Carlo (MC) titrations. The underlying theory is described in detail elsewhere.[44,48] For multiprotic systems, a pK_a value often cannot be attributed to a single group.[49] Instead, a protonation probability curve can describe the behavior of a group over the whole investigated pH range. However, this curve can deviate substantially from a Henderson–Hasselbalch curve. The theoretical framework used here allows to compute average interaction energies from the protonation probabilities obtained by the MC procedure.[44,48] The mean-field energy $G_{TR}^{\circ}(j_k, \mathrm{pH})$ of a particular titratable site j in its protonation form k (p for protonated and d for deprotonated) at a certain pH can be described by its intrinsic energy $G_{intr}(j_k)$ and its average interaction energy:[50,51]

$$G_{TR}^{\circ}(j_k, \mathrm{pH}) = G_{intr}(j_k) + \sum_{l \neq j}^{N_{site}} \sum_{m}^{N_{form,l}} G_{inter}(j_k, l_m) p(l_m, \mathrm{pH}) \quad (5)$$

The average interaction energy is the sum over all protonation forms m of all other sites l weighted by the probability p of form l_m at a given pH $p(l_m, \mathrm{pH})$ that we obtain from an MC calculation. Here, the number of sites of the system is given by N_{site}, and the number of protonation forms of site l is given by $N_{form,l}$. The averaging of this mean-field approach follows a similar spirit as the calculation of protonation probabilities based on the Tanford–Roxby iterative scheme.[52,53] Therefore, we call the pK_a values calculated based on the average interaction energies Tanford–Roxby pK_a values:

$$pK_{a,TR}(j, \mathrm{pH}) = -\frac{1}{RT\ln 10}\left(G_{TR}^{\circ}(j_p, \mathrm{pH}) - G_{TR}^{\circ}(j_d, \mathrm{pH})\right) \quad (6)$$

However, $pK_{a,TR}$ values are pH dependent. The free energy to protonate a site at a given pH can be estimated from this $pK_{a,TR}$ by:

$$G_{TR}(j, \mathrm{pH}) = RT\ln 10\left(\mathrm{pH} - pK_{a,TR}(j, \mathrm{pH})\right) \quad (7)$$

This energy is positive if the group is likely to be deprotonated and is negative if the group is likely to be protonated. Thus, from this energy, it can be seen how easily a group deprotonates or protonates at a given pH.

The intrinsic energy $G_{intr}(j_k)$ of a form j_k is composed of three contributions:

$$G_{intr}(j_k) = G_{model}(j_k) + \Delta G_{Born}(j_k) + \Delta G_{back}(j_k) \quad (8)$$

The model energy $G_{model}(j_k)$ represents the energy of form j_k inside a model compound in solution, which is usually determined experimentally. The Born energy difference $\Delta G_{Born}(j_k)$ characterizes the energy difference for polarizing the solvent around the protein and the model compound when the site j is charged from zero to its final charge in the protonation form j_k. The background energy difference $\Delta G_{back}(j_k)$ describes the interaction energy difference of form j_k with the charges of atoms not belonging to any site in the protein and in the model compound. The average interaction energy difference at a given pH is:

$$\Delta G_{TR,\mathrm{pH}}^{inter} = \sum_{l \neq j}^{N_{site}} \sum_{m}^{N_{form,l}} \left(G_{inter}(j_p, l_m) - G_{inter}(j_d, l_m)\right) p(l_m, \mathrm{pH}) \quad (9)$$

Computation of protonation probabilities and interaction energies

The electrostatic energies represented by the intrinsic energies $G_{intr}(j_k)$ and the interaction energies $G_{inter}(j_k, l_m)$ were calculated by programs based on the MEAD package.[44,54] The intrinsic energy values are calculated relative to experimentally determined pK_a values of appropriate model reactions of monoprotic compounds in aqueous solution.[48] For the semiquinone of FAD, we used a pK_a value of 8.5.[55] All residues of the types arginine, aspartate, glutamate, lysine, tyrosine, and histidine were

considered titratable. The following parameters were used in all Poisson–Boltzmann calculations: a dielectric constant of $\varepsilon_p = 4$ was assigned to the interior of the protein; the solvent was modeled as a medium with a dielectric constant of $\varepsilon_s = 80$, an ionic strength of $I = 100$ mM, and a temperature of $T = 300$ K. An ion exclusion layer of 2 Å and a solvent probe radius of 1.4 Å were used to define the volume of the protein. The electrostatic potential was calculated using a grid of 131^3 points, with two focusing steps at resolutions of 1.0 and 0.2 Å. The larger grid was geometrically centered on the molecule or complex, while the finer grid was geometrically centered on the group of interest.

The probabilities of all protonation forms j_k as a function of pH were calculated by a Metropolis MC algorithm.[56] pH was varied from 0 to 14 in steps of 0.2 pH unit. For every pH step, the MC calculation consisted of 100 equilibration scans and 10,000 production scans at $T = 300$ K. In one scan, each site of the protein is touched once on average.

Change in interaction energy between FNR and Fd

The change in interaction energy between FNR and Fd upon a change in the protonation or redox state of the isoalloxazine ring of the flavin, of the nicotinamide ring of NADP(H), of the side chain of Glu312, and of the iron–sulfur center of Fd was calculated as the sum of the respective interaction energies $G_{inter}(j_k, l_m)$. The flavin was included as oxidized (FAD), semiquinone ($FADH^{\cdot}$), or reduced ($FADH_2$); Fd was included as oxidized (Fd_{ox}) or reduced (Fd_{red}); and NADP(H) was included as $NADP^+$ or NADPH according to the proposed intermediates in the catalytic cycle.

Hydride-transfer energy

The hydride transfer from $FADH_2$ to $NADP^+$ catalyzed by FNR can be formally seen as a two-electron–two-proton reduction of $NADP^+$ and a two-electron–two-proton oxidation of $FADH_2$. A reduction potential of $E^{\circ\prime} = -323$ mV for the first reaction, as well as a reduction potential of $E^{\circ\prime} = -219$ mV for the second reaction, is measured at pH 7.0 in water ($I = 100$ mM; calculated from the *CRC Handbook of Chemistry and Physics*[20]). The total process:

$$FADH_2 + NADP^+ \rightarrow FAD + NADPH + H^+ \quad (10)$$

has therefore a reaction free energy of 4.8 kcal/mol in water. The role of the protein is to lower this free-energy difference to make the reaction possible. This effect is calculated by separately transferring the isoalloxazine ring of $FADH_2$ and FAD, as well as the nicotinamide ring of NADP+ and NADPH, from water to the protein environment. The calculation of these transfer energies is analogous to the calculation of relative protonation or reduction energies. The transfer energy consists of a difference in Born energy in water and in the protein, and an interaction energy with all titratable groups in the protein except for the flavin, NADP(H), and Glu312. Electronic polarization effects that could be considered in a self-consistent reaction field calculation have not been included in this study. Since the protonation state of the protein does not change upon the reaction, the titratable groups are kept fixed in their most probable protonation form. The interaction energies of the flavin, NADP(H), and Glu312 are included separately to avoid double counting of the contributions.

Acknowledgements

This work was supported by DFG grant UL174/7-1. V.I.D. is a fellow of CONICET, and N.C. is a staff member of the same institution. A fellowship from the Deutscher Akademischer Austauschdienst to V.I.D. is acknowledged. We are grateful to Dr. Néstor Carrillo for carefully reading the manuscript and to Dr. Eva-Maria Krammer for calculating the partial charges.

Supplementary Data

Supplementary data associated with this article can be found, in the online version, at doi:10.1016/j.jmb.2010.01.063

References

1. Avron, M. & Jagendorf, A. T. (1956). A TPNH diaphorase from chloroplasts. *Arch. Biochem. Biophys.* **65**, 475–490.
2. Shin, M. & Arnon, D. I. (1965). Enzymatic mechanisms of pyridine nucleotide reduction in chloroplasts. *J. Biol. Chem.* **240**, 1405–1411.
3. Arakaki, A. K., Ceccarelli, E. A. & Carrillo, N. (1997). Plant-type ferredoxin–$NADP^+$ reductases: a basal structural framework and a multiplicity of functions. *FASEB J.* **11**, 133–140.
4. Carrillo, N. & Ceccarelli, E. A. (2003). Open questions in ferredoxin–$NADP^+$ reductase catalytic mechanism. *Eur. J. Biochem.* **270**, 1900–1915.
5. Ceccarelli, E. A., Arakaki, A. K., Cortez, N. & Carrillo, N. (2004). Functional plasticity and catalytic efficiency in plant and bacterial ferredoxin–NADP(H) reductases. *Biochim. Biophys. Acta*, **1698**, 155–165.
6. Massey, V. (2000). The chemical and biological versatility of riboflavin. *Biochem. Soc. Trans.* **28**, 283–296.
7. Batie, C. J. & Kamin, H. (1984). Electron transfer by ferredoxin:$NADP^+$ reductase. Rapid reaction evidence for participation of a ternary complex. *J. Biol. Chem.* **259**, 11976–11985.
8. Batie, C. J. & Kamin, H. (1984). Ferredoxin:$NADP^+$ oxidoreductase. Equilibria in binary and ternary complexes with $NADP^+$ and ferredoxin. *J. Biol. Chem.* **259**, 8832–8839.
9. Bortolotti, A., Pérez-Dorado, I., Goñi, G., Medina, M., Hermoso, J. A., Carrillo, N. & Cortez, N. (2009). Coenzyme binding and hydride transfer in *Rhodobacter capsulatus* ferredoxin/flavodoxin NADP(H) oxidoreductase. *Biochim. Biophys. Acta*, **1794**, 199–210.
10. Hermoso, J. A., Mayoral, T., Faro, M., Gómez-Moreno, C., Sanz-Aparicio, J. & Medina, M. (2002). Mechanism of coenzyme recognition and binding revealed by crystal structure analysis of ferredoxin–$NADP^+$ reductase complexed with $NADP^+$. *J. Mol. Biol.* **319**, 1133–1142.
11. Humphrey, W., Dalke, A. & Schulten, K. (1996). VMD—Visual Molecular Dynamics. *J. Mol. Graphics*, **14**, 33–38.
12. Stone, J. (1998). *An Efficient Library for Parallel Ray Tracing and Animation*. Master's Thesis, Computer Science Department, University of Missouri-Rolla.
13. Bruns, C. M. & Karplus, P. A. (1995). Refined crystal

structure of spinach ferredoxin reductase at 1.7 Å resolution: oxidized, reduced and 2′-phospho-5′-AMP bound states. *J. Mol. Biol.* **247**, 125–145.
14. Kurisu, G., Kusunoki, M., Katoh, E., Yamazaki, T., Teshima, K., Onda, Y. *et al.* (2001). Structure of the electron transfer complex between ferredoxin and ferredoxin–$NADP^+$ reductase. *Nat. Struct. Biol.* **8**, 117–121.
15. Medina, M., Martinez-Júlvez, M., Hurley, J. K., Tollin, G. & Gómez-Moreno, C. (1998). Involvement of glutamic acid 301 in the catalytic mechanism of ferredoxin–$NADP^+$ reductase from *Anabaena* PCC 7119. *Biochemistry*, **37**, 2715–2728.
16. Aliverti, A., Deng, Z., Ravasi, D., Piubelli, L., Karplus, P. A. & Zanetti, G. (1998). Probing the function of the invariant glutamyl residue 312 in spinach ferredoxin–$NADP^+$ reductase. *J. Biol. Chem.* **273**, 34008–34015.
17. Baker, N. A., Sept, D., Joseph, S., Holst, M. J. & McCammon, J. A. (2001). Electrostatics of nanosystems: application to microtubules and the ribosome. *Proc. Natl Acad. Sci. USA*, **98**, 10037–10041.
18. DeLano, W. L. (2008). The PyMOL Molecular Graphics System DeLano Scientific, Palo Alto, CA, USA; http://www.pymol.org.
19. Persistence of Vision Raytracer Pty Ltd. POV-Ray. Persistence of Vision Raytracer Pty Ltd., PO Box 407, Williamstown, Victoria 3016, Australia. http://www.povray.org.
20. Vanýsek, P. (2004). Standard transformed Gibbs energy of formation for important biochemical species. In *CRC Handbook of Chemistry and Physics*, (Lide, R. C., ed), 85th edit. pp. 7–10, CRC Press, Boca Raton, FL.
21. Thompson, J. D., Higgins, D. G. & Gibson, T. J. (1994). CLUSTAL W: improving the sensitivity of progressive multiple sequence alignment through sequence weighting, position-specific gap penalties and weight matrix choice. *Nucleic Acids Res.* **22**, 4673–4680.
22. Shatsky, M., Nussinov, R. & Wolfson, H. J. (2004). A method for simultaneous alignment of multiple protein structures. *Proteins*, **56**, 143–156.
23. Shatsky, M., Nussinov, R. & Wolfson, H. J. (2006). Optimization of multiple-sequence alignment based on multiple-structure alignment. *Proteins*, **62**, 209–217.
24. Nogués, I., Pérez-Dorado, I., Frago, S., Bittel, C., Mayhew, S. G., Gómez-Moreno, C. *et al.* (2005). The ferredoxin–NADP(H) reductase from *Rhodobacter capsulatus*: molecular structure and catalytic mechanism. *Biochemistry*, **44**, 11730–11740.
25. Ingelman, M., Bianchi, V. & Eklund, H. (1997). The three-dimensional structure of flavodoxin reductase from *Escherichia coli* at 1.7 Å resolution. *J. Mol. Biol.* **268**, 147–157.
26. Sridhar Prasad, G., Kresge, N., Muhlberg, A. B., Shaw, A., Jung, Y. S., Burgess, B. K. & Stout, C. D. (1998). The crystal structure of NADPH:ferredoxin reductase from *Azotobacter vinelandii*. *Protein Sci.* **7**, 2541–2549.
27. Serre, L., Vellieux, F. M., Medina, M., Gomez-Moreno, C., Fontecilla-Camps, J. C. & Frey, M. (1996). X-ray structure of the ferredoxin:$NADP^+$ reductase from the cyanobacterium *Anabaena* PCC 7119 at 1.8 Å resolution, and crystallographic studies of $NADP^+$ binding at 2.25 Å resolution. *J. Mol. Biol.* **263**, 20–39.
28. Milani, M., Balconi, E., Aliverti, A., Mastrangelo, E., Seeber, F., Bolognesi, M. & Zanetti, G. (2007). Ferredoxin–$NADP^+$ reductase from *Plasmodium falciparum* undergoes $NADP^+$-dependent dimerization and inactivation: functional and crystallographic analysis. *J. Mol. Biol.* **367**, 501–513.
29. Deng, Z., Aliverti, A., Zanetti, G., Arakaki, A. K. & Ottado (1999). A productive $NADP^+$ binding mode of ferredoxin–$NADP^+$ reductase revealed by protein engineering and crystallographic studies. *Nat. Struct. Biol.* **6**, 847–853.
30. Dorowski, A., Hofmann, A., Steegborn, C., Boicu, M. & Huber, R. (2001). Crystal structure of paprika ferredoxin–$NADP^+$ reductase. Implications for the electron transfer pathway. *J. Biol. Chem.* **276**, 9253–9263.
31. Aliverti, A., Faber, R., Finnerty, C. M., Ferioli, C., Pandini, V., Negri, A. *et al.* (2001). Biochemical and crystallographic characterization of ferredoxin–$NADP^+$ reductase from nonphotosynthetic tissues. *Biochemistry*, **40**, 14501–14508.
32. Kabsch, W. (1978). A discussion of the solution for the best rotation to relate two sets of vectors. *Acta Crystallogr. Sect. A*, **34**, 827–828.
33. Brünger, A. T. & Karplus, M. (1988). Polar hydrogen positions in proteins: empirical energy placement and neutron diffraction comparison. *Proteins*, **4**, 148–156.
34. Brooks, B. R., Bruccoleri, R. E., Olafson, B. D., States, D. J., Swaminathan, S. & Karplus, M. (1983). CHARMM: a program for macromolecular energy, minimization, and dynamics calculations. *J. Comput. Chem.* **4**, 187–217.
35. MacKerell, A., Bashford, D., Bellott, M., Dunbrack, R., Evanseck, J., Field, M. *et al.* (1998). All-atom empirical potential for molecular modeling and dynamics studies of proteins. *J. Phys. Chem. B*, **102**, 3586–3616.
36. Pavelites, J. J., Bash, P. A., Gao, J. & MacKerell, J. A. D. (1997). A molecular mechanics force field for NAD^+, NADH, and the pyrophosphate groups of nucleotides. *J. Comput. Chem.* **18**, 221–239.
37. Bayly, C. I., Cieplak, P., Cornell, W. D. & Kollmann, P. A. (1993). A well-behaved electrostatic potential based method using charge restrains for deriving atomic charges: the RESP model. *J. Phys. Chem.* **97**, 10269–10280.
38. Frisch, M. J., Trucks, G. W., Schlegel, H. B., Scuseria, G. E., Robb, M. A., Cheeseman, J. R. *et al.* (2004). Gaussian 03, Revision C.02 Gaussian, Inc., Wallingford, CT.
39. Baerends, E. J., Autschbach, J., Bérces, A., Bickelhaupt, F. M., Bo, C., Boerrigter, P. M., et al. (2007). *ADF2007.01. SCM, Theoretical Chemistry*, Vrije Universiteit, Amsterdam, The Netherlands. http://www.scm.com.
40. te Velde, G., Bickelhaupt, F. M., Baerends, E. J., Guerra, C. F., van Gisbergen, S. J. A., Snijders, J. G. & Ziegler, T. (2001). Chemistry with ADF. *J. Comput. Chem.* **22**, 931–967.
41. Vosko, S. H., Wilk, L. & Nusair, M. (1980). Accurate spin-dependent electron liquid correlation energies for local spin density calculations: a critical analysis. *Can. J. Phys.* **58**, 1200.
42. Perdew, J. P. & Wang, Y. (1986). Accurate and simple density functional for the electronic exchange energy: generalized gradient approximation. *Phys. Rev. B*, **33**, 8800–8802.
43. Perdew, J. P., Chevary, J. A., Vosko, S. H., Jackson, K. A., Pederson, M. R., Singh, D. J. & Fiolhais, C. (1992). Atoms, molecules, solids, and surfaces: applications of the generalized gradient approximation for exchange and correlation. *Phys. Rev. B*, **46**, 6671–6687.
44. Essigke, T. (2008). *A Continuum Electrostatic Approach for Calculating the Binding Energetics of Multiple Ligands*. Ph.D. Thesis, University of Bayreuth. http://opus.ub.unibayreuth.de/volltexte/2008/410/.

45. Breneman, C. M. & Wiberg, K. B. (1990). Determining atom-centered monopoles from molecular electrostatic potentials. The need for high sampling density in formamide conformational analysis. *J. Comput. Chem.* **11**, 361–373.
46. Mouesca, J. M., Chen, J. L., Noodleman, L., Bashford, D. & Case, D. A. (1994). Density functional/Poisson–Boltzmann calculations of redox potentials for iron–sulfur clusters. *J. Am. Chem. Soc.* **116**, 11898–11914.
47. Ullmann, G. M., Noodleman, L. & Case, D. A. (2002). Density functional calculation of pK_a values and redox potentials in the bovine Rieske iron–sulfur protein. *J. Biol. Inorg. Chem.* **7**, 632–639.
48. Ullmann, G. M. & Knapp, E. W. (1999). Electrostatic models for computing protonation and redox equilibria in proteins. *Eur. Biophys. J.* **28**, 533–551.
49. Ullmann, G. M. (2003). Relations between protonation constants and titration curves in polyprotic acids: a critical view. *J. Phys. Chem. B*, **107**, 1263–1271.
50. Homeyer, N., Essigke, T., Ullmann, G. M. & Sticht, H. (2007). Effects of histidine protonation and phosphorylation on histidine-containing phosphocarrier protein structure, dynamics, and physicochemical properties. *Biochemistry*, **46**, 12314–12326.
51. Bombarda, E. & Ullmann, G. M. (2010). pH-dependent pKa values in proteins. A theoretical analysis of protonation energies with practical consequences for enzymatic reactions. *J. Phys. Chem.* **114**, 1994–2003.
52. Tanford, C. & Roxby, R. (1972). Interpretation of protein titration curves. Application to lysozyme. *Biochemistry*, **11**, 2192–2198.
53. Bashford, D. & Karplus, M. (1991). Multiple-site titration curves of proteins: an analysis of exact and approximate methods for their calculations. *J. Phys. Chem.* **95**, 9557–9561.
54. Bashford, D. & Karplus, M. (1990). pK_a's of ionizable groups in proteins: atomic detail from a continuum electrostatic model. *Biochemistry*, **29**, 10219–10225.
55. Mayhew, S. G. (1999). The effects of pH and semiquinone formation on the oxidation–reduction potentials of flavin mononucleotide. A reappraisal. *Eur. J. Biochem.* **265**, 698–702.
56. Metropolis, N. A., Rosenbluth, A. W., Rosenbluth, M. N., Teller, A. H. & Teller, E. (1953). Equation of state calculations by fast computing machines. *J. Chem. Phys.* **21**, 1087–1092.